JTE HCM-UTE
ISSN: 2615-9740

JOURNAL OF TECHNICAL EDUCATION SCIENCE
Ho Chi Minh City University of Technology and Engineering
Website: https://jte.edu.vn
Email: jte@hcmute.edu.vn

Paper-Based AgNW SEIRA Substrate for ppb-Level Detection of Carbendazim

Dinh Tuan Tran[+], Phuong Nhi T. Le[+], Hai Dang Ngo, Thi Kim Hang Pham[*]
Ho Chi Minh City University of Technology and Engineering, Vietnam

[*]Corresponding author. Email: hangptk@hcmute.edu.vn
[+]These authors contributed equally to this work.

ARTICLE INFO

Received: 17/09/2026
Revised: 30/09/2026
Accepted: 14/10/2026
Online First: 19/11/2026
Published:

KEYWORDS

Silver nanowire;
SEIRA;
Cellulose filter paper;
Carbendazim;
Localized surface plasmon resonance.

ABSTRACT

We report a surface-enhanced infrared absorption (SEIRA) substrate made of cellulose filter paper coated with silver nanowires (AgNWs) for the detection of carbendazim residues. AgNWs were synthesized by the polyol method, in which ethylene glycol acts as both solvent and reducing agent, polyvinylpyrrolidone as the morphology-directing agent, and Fe^{3+} ions as the selective oxidative etchant for crystal seeds. UV–Vis spectroscopy showed that a reaction time of 25 min gave the highest transverse/longitudinal plasmon peak intensity ratio (0.89), the most favorable condition for nanowire formation. SEM confirmed nanowires 454–6839 nm long and 39–85 nm in diameter, with a minor fraction of nanorods and nanoparticles. The substrate was prepared by three cycles of dipping and ultrasonication of the filter paper in the AgNW dispersion. On this substrate, the FTIR bands of carbendazim at 1280 cm^{-1} (ester C–O stretching) and 1644 cm^{-1} (benzimidazole C=N) were enhanced by factors of 1.4–9.3 in the ppm range and 4.5–9.4 in the ppb range, with detection down to 5 ppb. The low-cost, easily fabricated AgNW/filter-paper substrate is thus promising for rapid screening of trace pesticide residues.

DOI: https://doi.org/10.54644/jte.2026.2602

Copyright © JTE. This is an open-access article distributed under the terms and conditions of the Creative Commons Attribution-NonCommercial 4.0 International License which permits unrestricted use, distribution, and reproduction in any medium for non-commercial purpose, provided the original work is properly cited.

1. Introduction

Pesticides play an important role in maintaining the yield and quality of agricultural products, but the widespread and uncontrolled application of pesticides also causes the long-term presence of residues in agricultural products, soil and water sources, causing serious risks to human health and ecosystems [1]. Carbendazim, a broad-benzimidazole fungicide, is one of the most widely used active ingredients. It is used to control various fungal diseases in rice, fruit trees and vegetables. Carbendazim is relatively chemically stable and has the ability to build up in the environment. Toxicological studies have shown that this active substance may cause endocrine disruption, affect the ability to reproduce and cause liver damage in laboratory animals. Hence, many countries have established very strict maximum residue limits for carbendazim in agri-food products [2], [3]. Therefore, it is of great practical significance to develop rapid, sensitive and cost-effective methods for carbendazim residue detection.

The most common analytical techniques presently used for determination of carbendazim residues are high-performance liquid chromatography (HPLC) [4]-[6], liquid chromatography-tandem mass spectrometry (LC–MS/MS) [7]-[9] and gas chromatography-mass spectrometry (GC–MS) [10]. The techniques are very sensitive and selective but require expensive equipment, complex sample preparation, use of solvents, long analysis time, and must be performed in specialized laboratories by trained personnel. These limitations prevent them from fulfilling the requirement of rapid on-site screening of large sample volumes, which has led to the investigation of alternative analytical techniques based on surface-enhanced optical phenomena.

Fourier Transform Infrared (FTIR) spectroscopy provides information about the characteristic vibrations of functional groups and can identify molecules directly without labels. Nevertheless, the infrared absorption cross-section of a molecule is intrinsically small, complicating the detection of analytes at trace levels by standard FTIR. The SEIRA effect was first reported by Hartstein *et al*. in 1980, who observed that the infrared absorption of a molecular monolayer was amplified by several

orders of magnitude when it was covered with a thin metal overlayer [11]. The mechanism of the augmentation is mainly explained by electromagnetic factors. Localized surface plasmon resonance in metallic nanostructures generates a strong electromagnetic near field in the vicinity of the surface which enhances the interaction between infrared radiation and molecular vibrations. There are also chemical factors related to the interaction of molecules with the surface. The SEIRA effect is only effective for molecules situated near the metal surface because of the swift attenuation of the near field with distance, and the enhancement factor's magnitude is significantly influenced by the nanostructure's form, size, and hotspot density.

Among silver nanostructures, silver nanowires (AgNWs) are especially promising for SEIRA applications because of their high aspect ratio. The anisotropic structure gives rise to two distinct plasmon modes: a transverse mode in the UV–visible region and a longitudinal mode that strongly red-shifts with increasing length-to-diameter ratio, while at the same time concentrating a very strong electromagnetic field at both ends of the wire and at the junction points in the network. AgNW is normally prepared by the polyol process, where ethylene glycol functions as both the solvent and reducing agent, polyvinylpyrrolidone adsorbs selectively onto the {100} face to direct the growth along one axis, and a small amount of transition metal salts controls the oxidation etching process to maintain the five-fold twinned seed-the direct precursor of the nanowire [12]-[15]. This makes the position and the ratio of intensities between the two peaks of plasmon resonance a convenient tool to follow the process of wire formation directly from the UV–Vis spectrum [16]. The substrate choice also determines the feasibility of a practical SEIRA sensor. Cellulose filter paper is a promising candidate material because of its low cost, availability, and environmental friendliness, as well as its three-dimensional fibrous network structure with a large specific surface area, which facilitates the wide distribution of nanowires and the formation of many hotspots, whereas the natural capillarity of the paper also aids in enriching the analyte. Metal coated paper substrates have been demonstrated to be a viable platform for surface enhanced spectroscopy with some advantages in cost and field deployability as compared to photolithographically fabricated substrates [17], [18].

This study first synthesizes AgNWs by an $FeCl_3$-assisted polyol method and examines the effect of reaction time on wire formation using UV–Vis absorption spectra. Second, a SEIRA substrate is fabricated by coating the AgNWs onto cellulose filter paper through repeated dipping and ultrasonication, and its morphology is examined by SEM. Third, the FTIR signal enhancement of carbendazim on the substrate is evaluated from the ppm to the ppb range using the enhancement factors of two characteristic vibrational bands, thereby assessing the potential application of the substrate in rapid screening of pesticide residues.

2. Materials and Methods

2.1. Chemicals and materials

The chemicals used in the study include: ethylene glycol (EG), polyvinylpyrrolidone (PVP), silver nitrate ($AgNO_3$), iron(III) chloride ($FeCl_3$), carbendazim, ethanol, and deionized water (DI). The substrate is cellulose filter paper.

2.2. Synthesis of silver nanowires by the polyol method

Silver nanowires were synthesized using the polyol method, in which EG simultaneously acts as a solvent and a reducing agent for Ag^+ ions, PVP serves as a morphology directing agent by selectively adsorbing onto the {100} crystal face of silver, while Fe^{3+} and Cl^- ions from $FeCl_3$ control the oxidative etching process to remove single crystal seeds and maintain five-fold twinned polycrystalline seeds, the precursor of the nanowires [12]-[15]. The process consists of three steps:

Step 1: 36 mL of EG and 0.0716 g of PVP (pre-dissolved in 4 mL of EG) were added to a three-neck flask, heated to 140°C, and held for 75 minutes on a magnetic stirrer to remove adsorbed water and stabilize the solution.

Step 2: Preparation of the oxidative etching environment. The system temperature was raised to 160°C and maintained for 15 minutes to ensure thermal stabilization. Subsequently, 400 µL of a 4×10^{-3} M $FeCl_3$ solution was added to the reaction vessel, and the mixture was continuously stirred

for 40 minutes to establish an oxidative etching environment prior to the introduction of the silver precursor.

Step 3: Addition of the silver precursor. $AgNO_3$ (0.2294 g), previously dissolved in 4 mL of EG, was slowly added to the reaction mixture. The color change of the solution from light yellow to metallic gray was monitored as a qualitative indication of the formation and growth of silver nanostructures. Aliquots were collected at reaction times of 15, 20, 25, 30, 35, 40, 45, and 50 minutes, rapidly cooled to room temperature, and stored in dark glass vials.

2.3. Fabrication of SEIRA AgNW substrate on cellulose filter paper

The SEIRA substrate is fabricated using a dip-coating method combined with ultrasonic shaking on a cellulose filter paper substrate, following the sequence below:

Step 1: Prepare the paper base: Tweezers and scissors are cleaned with ethanol to avoid contaminating the filter paper. The filter paper is cut into pieces measuring 1 cm × 1.5 cm.

Step 2: Cleaning the silver solution: The AgNW solution after synthesis is centrifuged multiple times with DI water to remove excess EG, free PVP, and residual ions from the reaction process, then redispersed in DI water.

Step 3: Coating with silver nanowires: The filter paper base is directly immersed in the AgNW solution and sonicated for 5 minutes, then removed and allowed to air dry for at least 30 minutes. The immersion-ultrasonic shaking-drying cycle is repeated three times to increase the amount of silver nanowires adhering to the paper substrate. The base, after completely drying, is stored in a glass jar, avoiding direct sunlight.

2.4. Characterization of AgNW Substrates and carbendazim Detection

The optical characteristics of the AgNW dispersions were characterized by UV–Vis absorption spectroscopy over 300–600 nm . The morphology, size, and distribution of silver nanowires on filter paper were investigated using scanning electron microscopy (SEM); the length and diameter of the structures were statistically analyzed from SEM images. The vibrational signal of carbendazim was recorded using Fourier-transform infrared spectroscopy (FTIR).

3. Results and Discussions

3.1. UV – Vis spectrum of Ag nanowires

Figure 1 presents the UV–Vis absorption spectra of the Ag nanowire samples in the range of 300–600 nm wavelength. The results show that all samples exhibit a strong absorption region between 351 and 383 nm, characteristic of surface plasmon resonance in silver nanostructures, a phenomenon arising from the collective oscillation of conduction electrons on the Ag surface under electromagnetic radiation. For Ag nanowires, the position and shape of the absorption band depend significantly on the size, morphology, aspect ratio (length-to-diameter ratio), and dispersion state of the wires.

For Ag nanowire structures, plasmon oscillations can be categorized into two main components: transverse and longitudinal oscillations. Transverse oscillations typically appear in the 350–351 nm wavelength range, whereas longitudinal oscillations appear at longer wavelengths, around 380–383 nm. As the wire length or the aspect ratio (length-to-diameter ratio) increases, the longitudinal plasmon oscillation shifts toward longer wavelengths due to changes in electronic polarization along the wire axis [16].

Furthermore, the position and intensity of the absorption peaks vary depending on the synthesis conditions. Changes in reaction time reveal distinct optical characteristics corresponding to three stages of silver nanowire formation: nucleation, growth, and degradation [13]. During the nucleation stage (15 minutes of reduction), only the peak characteristic of Ag nanoparticles appears. The growth stage (20–30 minutes) exhibits two plasmon resonance peaks: one at 350–351 nm and another at 380–383 nm, where the former corresponds to transverse plasmon oscillation absorption and the latter to longitudinal plasmon oscillation absorption. Finally, the degradation stage (35–50 minutes) marks the point where the silver nanowires begin to degrade or reach saturation, likely because the majority of silver ions have been consumed, thereby slowing the wire growth rate.

JTE
HCM-UTE
ISSN: 2615-9740

JOURNAL OF TECHNICAL EDUCATION SCIENCE
Ho Chi Minh City University of Technology and Engineering
Website: https://jte.edu.vn
Email: jte@hcmute.edu.vn

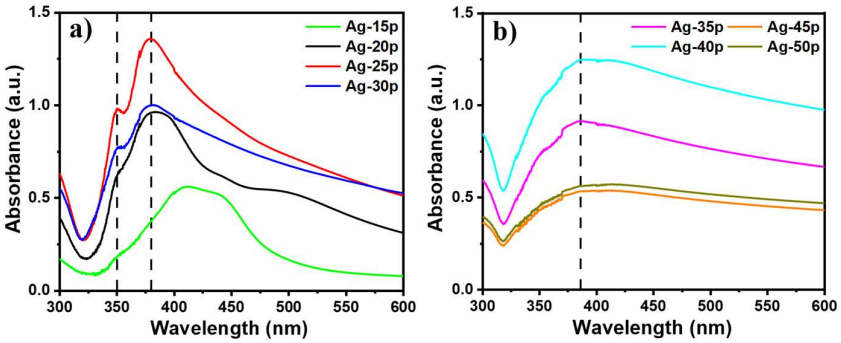


Figure 1. *UV–Vis absorption spectra of Ag nanowires samples collected at reaction times of (a) 15–30 min and (b) 35–50 min.*

The AgNW/AgNP peak ratios are presented in Table 1; the lowest ratio was 0.64 at a reaction time of 20 minutes, while the highest was 0.89 at 25 minutes. The ratio increased from 0.64 to 0.89 as the reaction time extended from 20 to 25 minutes, then decreased to 0.76 at 30 minutes. Thus, a reaction time of 25 minutes yielded the highest intensity ratio between the two plasmon resonance peaks (0.89), representing the most favorable condition for silver nanowire formation within the range investigated.

Table 1. *Peak ratios between wire-like and particle-like Ag structures.*

Reaction time	Peak at ~350 nm (A)	Peak of ~380 nm (B)	Ratio of A/B
20 min	0.61–351 nm	0.95–380 nm	0.64
25 min	0.97–350 nm	1.087–383 nm	0.89
30 min	0.76–350 nm	1.0–380 nm	0.76

3.2. Surface morphology of AgNWs via SEM images

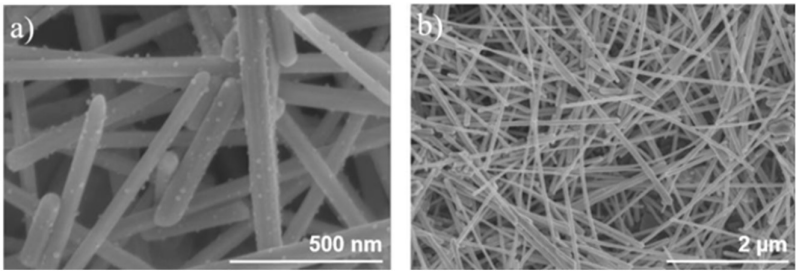


Figure 2. *SEM image of AgNWs at a) high and b) magnification.*

Table 2. *Dimensions of AgNWs and silver nanorods (AgNRs) measured from SEM images.*

Structure	Length (nm)	Diameter (nm)
AgNW	454–6839	39–85
AgNR	110–632	50–104

Figure 2 illustrates the surface morphology of the synthesized silver nanomaterials. At high magnification (500 nm scale bar), silver nanowires and nanorods with smooth surfaces are clearly visible, alongside a small number of scattered spherical nanoparticles. At a wider field of view (2 µm), the nanowires appear densely distributed and interwoven into a relatively uniform network, free of large agglomerates, a configuration that facilitates the formation of numerous inter-wire junctions. The dimensions of AgNWs are presented in Table 2. Statistical analysis of the SEM images reveals that the silver nanowires range from 454 to 6839 nm in length and from 39 to 85 nm in diameter, corresponding to aspect ratios ranging from approximately 11 to more than 80. Additionally, the sample contains shorter nanorods, with lengths of 110–632 nm and diameters of 50–104 nm. The coexistence of

nanowires, nanorods, and nanoparticles indicates that the synthesis process was not entirely morphologically selective, although nanowires remain the dominant structure. These results are consistent with the plasmon absorption characteristics observed in the UV–Vis spectra: the peak in the short wavelength region corresponds to transverse plasmon oscillation, whereas the peak in the longer wavelength region appears only for anisotropic silver structures with high aspect ratios, specifically silver nanowires.

3.3. Surface morphology via SEM image of AgNWs coated on a filter paper substrate

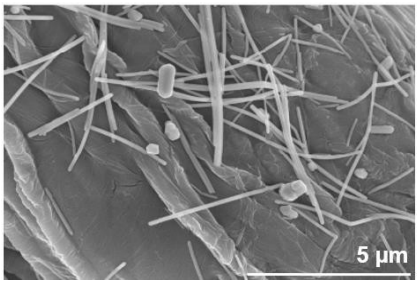


Figure 3. *SEM image of Ag nanowires deposited on a filter paper substrate.*

Figure 3 presents SEM images of the filter paper substrate after silver nanowire coating, intended to evaluate the morphology and distribution of the nanomaterials on the support matrix. The images clearly reveal the characteristic cellulose fiber network of the filter paper, featuring a relatively rough surface and voids between the fibers.

Silver nanowires and nanorods are distributed across the entire substrate surface; some adhere along the axes of the cellulose fibers, while others penetrate the voids between them. Consequently, the silver nanomaterials are not confined to the surface layer but are distributed within the paper's three–dimensional network structure, a configuration that facilitates a higher density of electromagnetic hotspots and an increased effective contact area with analyte molecules. Additionally, polyhedral structures ranging from 302 to 954 nm in size were observed, indicating the presence of a minor secondary phase in the product.

Statistical analysis of the SEM images indicates that the silver nanowires on the substrate have lengths of 2791–8136 nm and diameters of 70–178 nm, dimensions that exceed those measured in the initial solution samples (454–6839 nm and 39–85 nm). This discrepancy may be attributed to the loss of shorter wires during the purification centrifugation and the immersion-sonication cycles, as well as the tendency for adjacent wires on the cellulose fibers to be measured as a single unit during diameter analysis. These results demonstrate that the combined immersion and ultrasonic vibration process enables the coating of filter paper with silver nanowires at a density and coverage suitable for use as a SEIRA substrate.

3.4. FTIR spectrum of Carbendazim on an AgNW-loaded filter paper substrate at ppm levels

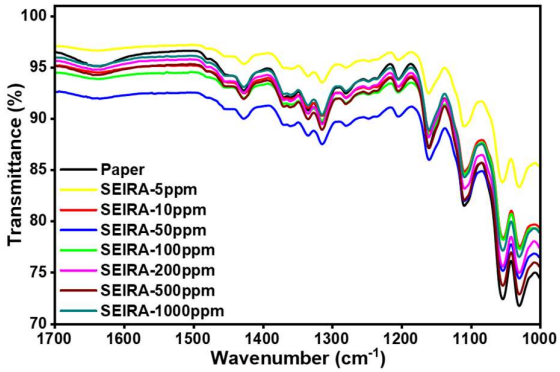


Figure 4. *FTIR spectra of carbendazim (5–1000 ppm) on the AgNW/filter-paper SEIRA substrate and of bare filter paper.*

Table 3. *Enhancement factors (EF) of carbendazim bands on the AgNW SEIRA substrate at ppm concentrations.*

Concentration	Peak position (cm^{-1})	Ag/Paper
1000 ppm	1280 C–O	4.00
	1644 C=N	4.51
500 ppm	1280 C–O	6.64
	1644 C=N	8.54
200 ppm	1280 C–O	5.95
	1644 C=N	6.22
100 ppm	1280 C–O	2.99
	1644 C=N	3.80
50 ppm	1280 C–O	6.44
	1644 C=N	9.34
10 ppm	1280 C–O	3.16
	1644 C=N	4.16
5 ppm	1280 C–O	1.44
	1644 C=N	1.74

Figure 4 presents the FTIR spectra of carbendazim at concentrations ranging from 1000 ppm to 5 ppm on an AgNW/filter paper SEIRA substrate. EF = A_{SEIRA} / A_{paper}, where A is the baseline-corrected absorbance of the same band on the AgNW substrate and on bare filter paper. The two peaks selected for signal monitoring were 1644 cm^{-1}, corresponding to the benzimidazole ring skeleton vibration (C=N), and 1280 cm^{-1}, characteristic of the ester group stretching vibration (C–O). These two vibrations exhibit strong intensities and are distinct from the cellulose substrate's absorption bands, making them favorable for quantitative comparison. The enhancement factors at the investigated concentrations are summarized in Table 3. At 1000 ppm, the enhancement factor reached 4.00 at the 1280 cm^{-1} peak and 4.51 at the 1644 cm^{-1} peak; at 5 ppm, the corresponding values decreased to 1.44 and 1.74. Throughout the investigated range, the enhancement factor at the 1644 cm^{-1} peak was consistently higher than that at 1280 cm^{-1}, indicating that the C=N vibration of the benzimidazole skeleton was enhanced more effectively than the C–O vibration of the ester group. It is noteworthy that the enhancement factor did not decrease monotonically with concentration but fluctuated between 1.44 and 9.34, with the highest values recorded at 50 ppm (6.44 and 9.34) rather than at the highest concentration. This trend aligns with the nature of the SEIRA effect: the enhanced signal originates only from the molecular layer within the near-field region of the silver nanowires; consequently, at high concentrations, the majority of molecules lie outside this region and contribute to the background signal rather than the enhanced signal, thereby reducing the apparent enhancement factor. Conversely, as the concentration decreases, the proportion of molecules adsorbed close to the surface increases, yet the absolute signal weakens and measurement errors rise. Thus, the SEIRA AgNW/filter paper substrate maintains its ability to enhance the FTIR signal of carbendazim across the entire investigated ppm concentration range, demonstrating potential for the detection of trace amounts of pesticides.

3.5. FTIR spectrum of Carbendazim on an AgNW-loaded filter paper substrate at ppb levels

Figure 5 presents the FTIR spectra of carbendazim in the ppb concentration range on the AgNW/filter paper SEIRA substrate, with the corresponding enhancement factors summarized in Table 4. Even when the concentration was reduced by three orders of magnitude compared to the ppm range, two characteristic peaks at 1280 cm^{-1} and 1644 cm^{-1} remained clearly detectable. At 1000 ppb, the enhancement factors reached 5.99 and 4.74; at the lowest concentration investigated (5 ppb), the

corresponding values remained at 8.11 and 8.80. Thus, the substrate enables the detection of carbendazim at concentrations as low as 5 ppb.

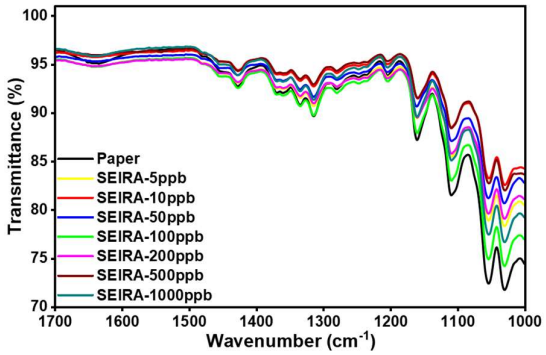


Figure 5. *FTIR spectra of carbendazim (5–1000 ppb) on the AgNW/filter-paper SEIRA substrate and of bare filter paper.*

Table 4. *Enhancement factors (EF) of carbendazim bands on the AgNW SEIRA substrate at ppb concentrations.*

Concentration	Peak position (cm^{-1})	Ag/Paper
1000 ppb	1280 C–O	5.99
	1644 C=N	4.74
500 ppb	1280 C–O	19.39
	1644 C=N	10.24
200 ppb	1280 C–O	6.10
	1644 C=N	5.95
100 ppb	1280 C–O	8.94
	1644 C=N	8.25
50 ppb	1280 C–O	15.09
	1644 C=N	14.07
10 ppb	1280 C–O	4.46
	1644 C=N	5.48
5 ppb	1280 C–O	8.11
	1644 C=N	8.80

Notably, the enhancement factors in the ppb range varied widely between 4.5 and 19.4 and did not decrease with concentration. The highest values were recorded at 500 ppb (19.39 and 10.24) and 50 ppb (15.09 and 14.07). This trend is consistent with observations in the ppm range and reflects the surface-specific nature of the SEIRA effect: the enhanced signal originates solely from the molecular layer within the near-field region of the silver nanowires; consequently, the enhancement factor reflects the proportion of molecules adsorbed near the surface rather than the total amount of analyte on the substrate. Furthermore, at very low concentrations, the weak absolute signal renders the enhancement factor sensitive to baseline fluctuations and the non-uniform distribution of hotspots across measurement sites. The enhancement mechanism on the AgNW/filter paper substrate can be attributed to two contributing factors. The dominant contribution is the electromagnetic effect: localized surface plasmon resonance on the silver nanowires generates an intense near-field-strongly concentrated at the wire ends and at network junctions-which amplifies the interaction between infrared radiation and molecular vibrations. Since the near-field intensity decays rapidly with distance, only molecules located in the immediate vicinity of the metal surface experience enhancement; this is why the analyte's adsorption

capability determines SEIRA efficiency. A second factor involves the PVP layer remaining on the nanowire surface following synthesis. The carbonyl groups of PVP can form hydrogen bonds with the N–H groups of carbendazim and engage in dipole-dipole interactions with the nitrogen and oxygen atoms within the molecule, thereby retaining the analyte near the AgNW surface rather than allowing it to disperse freely within the cellulose matrix. Consequently, the role of PVP is twofold: i) it facilitates the anchoring of molecules within the near-field region; ii) it creates a buffer layer that increases the molecule-metal separation distance, thereby limiting the achievable enhancement.

4. Conclusions

A SEIRA substrate based on cellulose filter paper coated with silver nanowires (AgNWs) was successfully fabricated using a process combining immersion and ultrasonic vibration. The AgNWs were synthesized via an $FeCl_3$-assisted polyol method; UV–Vis spectral analysis identified a 25-minute reaction time as optimal, yielding an intensity ratio of 0.89 between the two plasmon resonance peaks. SEM images showed AgNWs 454–6839 nm long and 39–85 nm in diameter in the dispersion; on the paper substrate, the wires (2791–8136 nm long, 70–178 nm in diameter) were distributed across the surface and between cellulose fibers to form a network with a high density of intersection points.

Using the fabricated substrate, the FTIR signals of carbendazim at the characteristic peaks of 1280 cm^{-1} (C–O) and 1644 cm^{-1} (C=N) were significantly enhanced; enhancement factors ranged from 1.4 to 9.3 in the ppm range and 4.5 to 19.4 in the ppb range, enabling the detection of carbendazim at concentrations as low as 5 ppb. This enhancement effect is attributed to localized surface plasmon resonance on the AgNWs, combined with the role of the PVP layer in retaining analyte molecules near the surface.

With low production costs and a simple fabrication process, the AgNW/cellulose filter paper SEIRA substrate demonstrates potential for the rapid screening of pesticide residues. Future studies should evaluate signal reproducibility, establish quantitative calibration curves and limits of detection, and conduct testing on actual agricultural produce samples.

Acknowledgments

This work was supported by Project No. SV2026-62, funded by Ho Chi Minh City University of Technology and Engineering, Vietnam.

Conflict of Interest

The authors declare no conflict of interest.

Declaration of generative AI and AI-assisted technologies in the writing process

During the preparation of this work, the authors used ChatGPT for editing in the English language. The authors reviewed and edited the content as needed and take full responsibility for the content of the publication after using this tool.

Data Availability Statement

The data that support the findings of this study are available from the corresponding author upon reasonable request.

REFERENCES

[1] C. A. Damalas and I. G. Eleftherohorinos, “Pesticide exposure, safety issues, and risk assessment indicators,” *Int. J. Environ. Res. Public Health*, vol. 8, no. 5, pp. 1402–1419, May 2011, doi: 10.3390/ijerph8051402.

[2] S. Singh *et al.*, “Toxicity, monitoring and biodegradation of the fungicide carbendazim,” *Environ. Chem. Lett.*, vol. 14, no. 3, pp. 317–329, Sep. 2016, doi: 10.1007/s10311-016-0566-2.

[3] European Food Safety Authority (EFSA), “Updated reasoned opinion on the toxicological properties and maximum residue levels (MRLs) for the benzimidazole substances carbendazim and thiophanate-methyl,” *EFSA J.*, vol. 22, no. 2, p. e8569, Feb. 2024, doi: 10.2903/j.efsa.2024.8569.

[4] M. Michel and B. Buszewski, “Optimization of a matrix solid-phase dispersion method for the determination analysis of carbendazim residue in plant material,” *J. Chromatogr. B*, vol. 800, no. 1–2, pp. 309–314, 2004, doi: 10.1016/j.jchromb.2003.08.039.

[5] X. Qin *et al.*, “Determination of carbendazim and diethofencarb in cotton and soil by high-performance liquid chromatography,” *Anal. Lett.*, vol. 49, no. 10, pp. 1631–1639, Jan. 2016, doi: 10.1080/00032719.2015.1116006.

[6] M. Akkbik and O. Hazer, "Novel molecularly imprinted polymer for the determination of carbendazim from water and food by solid-phase extraction and high-performance liquid chromatography," *Anal. Lett.*, vol. 51, no. 1–2, pp. 7–23, Jan. 2018, doi: 10.1080/00032719.2017.1284859.
[7] S. Grujic *et al.*, "Determination of carbendazim residues in fruit juices by liquid chromatography–tandem mass spectrometry," *Food Addit. Contam.*, vol. 22, no. 11, pp. 1132–1137, Nov. 2005, doi: 10.1080/02652030500352863.
[8] K. A. Bean and J. D. Henion, "Determination of carbendazim in soil and lake water by immunoaffinity extraction and coupled-column liquid chromatography–tandem mass spectrometry," *J. Chromatogr. A*, vol. 791, no. 1–2, pp. 119–126, Dec. 1997, doi: 10.1016/S0021-9673(97)00819-4.
[9] X. Xu *et al.*, "Carbendazim residues in vegetables in China between 2014 and 2016 and a chronic carbendazim exposure risk assessment," *Food Control*, vol. 91, pp. 20–25, Mar. 2018, doi: 10.1016/j.foodcont.2018.03.016.
[10] M. O. Almeida *et al.*, "Optimization of method for pesticide detection in honey by using liquid and gas chromatography coupled with mass spectrometric detection," *Foods*, vol. 9, no. 10, p. 1368, Sep. 2020, doi: 10.3390/foods9101368.
[11] A. Hartstein *et al.*, "Enhancement of the infrared absorption from molecular monolayers with thin metal overlayers," *Phys. Rev. Lett.*, vol. 45, no. 3, pp. 201–204, Jul. 1980, doi: 10.1103/PhysRevLett.45.201.
[12] B. Wiley *et al.*, "Polyol synthesis of silver nanostructures: Control of product morphology with Fe(II) or Fe(III) species," *Langmuir*, vol. 21, no. 18, pp. 8077–8080, Aug. 2005, doi: 10.1021/la050887i.
[13] Y. Sun and Y. Xia, "Large-scale synthesis of uniform silver nanowires through a soft, self-seeding, polyol process," *Adv. Mater.*, vol. 14, no. 11, pp. 833–837, Jun. 2002, doi: 10.1002/1521-4095(20020605)14:11<833::AID-ADMA833>3.0.CO;2-K.
[14] Y. Sun *et al.*, "Polyol synthesis of uniform silver nanowires: A plausible growth mechanism and the supporting evidence," *Nano Lett.*, vol. 3, no. 7, pp. 955–960, Jun. 2003, doi: 10.1021/nl034312m.
[15] N. M. Abbasi *et al.*, "Preparation of silver nanowires and their application in conducting polymer nanocomposites," *Mater. Chem. Phys.*, vol. 166, pp. 1–15, Sep. 2015, doi: 10.1016/j.matchemphys.2015.08.056.
[16] M. N'Gom *et al.*, "Single particle plasmon spectroscopy of silver nanowires and gold nanorods," *Nano Lett.*, vol. 8, no. 10, pp. 3200–3204, Oct. 2008, doi: 10.1021/nl801504v.
[17] W. W. Yu and I. M. White, "Inkjet printed surface enhanced Raman spectroscopy array on cellulose paper," *Anal. Chem.*, vol. 82, no. 23, pp. 9626–9630, Dec. 2010, doi: 10.1021/ac102475k.
[18] C. H. Lee *et al.*, "Paper-based SERS swab for rapid trace detection on real-world surfaces," *ACS Appl. Mater. Interfaces*, vol. 2, no. 12, pp. 3429–3435, Dec. 2010, doi: 10.1021/am1009875.

Dinh Tuan Tran is currently a final-year student majoring in Materials Technology at Ho Chi Minh City University of Technology and Engineering (HCM-UTE), Vietnam. The author's research interests include silver nanomaterials (Ag) and their applications in detecting organic residues.
Email: 22130025@student.hcmute.edu.vn. ORCID: https://orcid.org/0009-0000-2533-8014.

Phuong Nhi T. Le is currently a final-year student majoring in Materials Technology at Ho Chi Minh City University of Technology and Engineering (HCM-UTE), Vietnam. The author's research interests are not specified in the provided biography.
Email: 23130037@student.hcmute.edu.vn. ORCID: https://orcid.org/0009-0005-9544-0854.

Hai Dang Ngo received the M.S. degree from Ajou University, Suwon, South Korea, and the Ph.D. degree from Hokkaido University, Sapporo, Japan. The author is affiliated with Ho Chi Minh City University of Technology and Engineering, Vietnam. The author's research interests include the optical and electrical properties of thin films and low-dimensional systems.
Email: dangnh@hcmute.edu.vn. ORCID: https://orcid.org/0000-0002-6205-0850.

Thi Kim Hang Pham received the M.S. degree from the Institute of Physics, Hanoi, Vietnam, in 2011, and the Ph.D. degree from Ewha Womans University, South Korea, in 2019. The author has experience in the fabrication and characterization of magnetic and semiconductor materials using physical deposition techniques.
Email: hangptk@hcmute.edu.vn. ORCID: https://orcid.org/0009-0000-4865-3420.